

Friction on layered media: How deep do phonons reach?

Miru Lee,^{1,*} Niklas Weber,² Cynthia A. Volkert,² and Matthias Krüger^{1,†}

¹*Institute for Theoretical Physics, Georg-August-Universität Göttingen, 37073 Göttingen, Germany*

²*Institute of Materials Physics, Georg-August-Universität Göttingen, 37073 Göttingen, Germany*

(Dated: May 24, 2023)

We theoretically study the frictional damping of a small probe object on a coated planar surface, analyzing the resulting phonon modes via a theory of viscoelasticity. Three different types of excitations are found to contribute to friction in distinct ways: traveling (3D) spherical waves, traveling (2D) surface waves, and evanescent waves. While traveling waves transport energy away from the probe, determined by long range elastic properties (wavelength), evanescent waves transform energy into heat in a near-field range, characterized by the size of the probe. Thus, fundamentally different behaviors are predicted, depending on coating thickness and material properties.

Sliding friction is a complex phenomenon, involving surface mechanics [1–8] and production of heat in the surrounding media. In the latter process, the relevant degrees of freedom have been found to include electronic [9–13] and phononic ones [8, 11–23]. The role of phonon modes can be isolated by tuning them while keeping the surface properties and contact mechanics unchanged. This has been achieved by inducing a phase transition in the solid [13, 19], or by changing an external electric field [20].

Studying friction on layers of different thickness is another way of achieving this goal; it is especially insightful as it not only allows material properties to be tailored while limiting changes in the contact surface, it also reveals how deep friction feels into the material. Many numerical and nanoscale experimental studies have been done on the effect of layers [24–36], with a variety of interesting behaviors. For example, while adding graphene layers between sliding bodies can substantially reduce friction [33], both increases [24–26] and decreases [27, 30–32] in friction have been observed as the number of graphene layers is increased. Friction has also been observed to decrease with thickness for other layered materials, such as molybdenum disulfide and niobium diselenide, when they are weakly anchored to the substrate [32]. A numerical study, in contrast, found that friction increases with thickness, when the bottom layer absorbs incoming phonons [34]. Additionally, it has been reported that friction is smaller for strongly anchored samples compared to weakly anchored ones, suggesting that the changes in friction could be results of changes in local deformations [28, 29, 36]. The complexity of the observed behavior calls for a theoretical analysis that systematically addresses the dependence of phononic damping on layer thickness, boundary conditions, and material properties.

In this manuscript, we analyze friction of a nanoscopic object on a 3D planar coated substrate, treating phonon modes via a field theory of viscoelasticity that includes phonon attenuation. We find that friction arises due to traveling spherical waves, cylindrical surface waves, or evanescent waves, each dominating in different regimes of

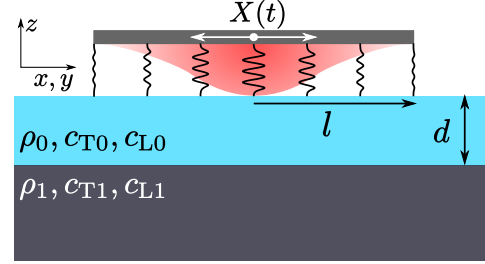


FIG. 1. Investigated system: a probe is coupled to the surface of a coated substrate, and oscillates parallel to it. The coupling interaction carries an interaction radius l . The coating of thickness d and the substrate are characterized by mass density ρ and transverse (c_T) and longitudinal (c_L) speeds of sound, as indicated.

material properties and coating thickness. A finite viscosity thus not only results in phonon attenuation, but also, here more importantly, in losses from evanescent waves. Consequently, friction shows drastically different dependencies on coating thickness ranging from short range to long range behavior, and can increase or decrease with coating thickness. These regimes are determined by the phonon attenuation coefficients and the refractive index.

Consider a probe coupled to an isotropic solid filling the space $z \leq 0$ (see Fig. 1). The probe oscillates parallel to the surface, so that its x coordinate is $X(t) = \text{Re}\{X_0 e^{i\omega t}\}$. The coupling with the surface causes a force acting on the probe, whose x -coordinate is $F(t) = \text{Re}\{F_0 e^{i\omega t}\}$. The damping coefficient or friction coefficient of the probe Γ is defined as $\Gamma = \omega^{-1} \text{Im}\{F_0/X_0\}$ [37]

The specific form of coupling is not important for the conclusions of this manuscript, as detailed in the Supplemental Material (SM). We thus use a simple linear one, which allows us to find analytic expressions,

$$F(t) = n_A \kappa \iint_{-\infty}^{\infty} d^2 \mathbf{r}_{\parallel} (-X(t) + u_x(\mathbf{r}_{\parallel}, t)) e^{-\frac{r_{\parallel}^2}{l^2}}, \quad (1)$$

where $\mathbf{r}_{\parallel} = (x, y, 0)$ marks a position on the surface, and $u_x(\mathbf{r}_{\parallel}, t)$ is the x -component of the phonon field at $z = 0$

(introduced below). n_A is the particle number per unit area [38], and κ is the coupling strength. Equation (1) contains a Gaussian envelope of width l , introducing a length scale of the interaction range or probe size.

The first term in Eq. (1) is the force in absence of phonon excitations; it is in phase with $X(t)$ and does not contribute to the damping coefficient Γ . The second term is the force due to excitations of the phonon field \mathbf{u} , treated via a theory of viscoelasticity, i.e., using a Kelvin-Voigt model [39–42],

$$(c_L^2 - c_T^2) \nabla \nabla \cdot \mathbf{u}(\mathbf{r}, \omega) + c_T^2 \nabla^2 \mathbf{u}(\mathbf{r}, \omega) = -\omega^2 \mathbf{u}(\mathbf{r}, \omega). \quad (2)$$

The coupling to the probe enters Eq. (2) via a time dependent boundary condition. The resulting solution for u_x contains a part that is phase shifted with respect to $X(t)$, yielding the damping coefficient Γ [16, 17]. The oscillating probe excites phonons, whereby its motion is damped. The solution of this problem proceeds via the Green's function of Eq. (2) (SM).

Equation (2) is a widely applicable model of phonon dynamics [39–41], and related models have been influential in understanding friction [16, 18]. It contains two fundamental modes with longitudinal, $c_L(\omega) = \sqrt{\frac{3K+4\mu-i\omega(3\xi+4\eta)}{3\rho}}$, and transverse, $c_T(\omega) = \sqrt{\frac{\mu-i\omega\eta}{\rho}}$, speeds of sound. K and μ (ξ and η) are the bulk and shear elastic (viscous) moduli, respectively, and ρ the mass density. c_T and c_L are complex due to finite viscous moduli, i.e., Eq. (2) contains phonon attenuation. Microscopically, such attenuation may be caused by phonon-phonon, phonon-electron, or phonon-defect scattering. For simplicity, we assume $c_L(\omega)/c_T(\omega) = \sqrt{3}$, independent of ω , a good approximation for solids [16, 43–45]. c_L thus drops out of the discussion.

The bulk situation, where the coating thickness d in Fig. 1 is infinite, was extensively studied previously [16, 17, 42, 46]. In this case, the probe excites spherical waves $\sim e^{i\omega r_{\parallel}/c_{T0}}/r_{\parallel}$ (SM), and the damping coefficient reads

$$\Gamma^\infty = \frac{\kappa^2 n_A^2 l^4}{c_{T0}^3 \rho_0} \left(\zeta^{\text{ela}} + \frac{\zeta^{\text{vis}} \eta_0}{c_{T0}^3 \rho_0 l} + \mathcal{O}\left(\frac{1}{Q^2}, \frac{l^2}{\lambda^2}\right) \right), \quad (3)$$

with $\zeta^{\text{ela}} \approx 1.29$, $\zeta^{\text{vis}} \approx 1.72$, and c_{T0} the real part of c_{T0} . Eq. (3) is valid for $l \ll \lambda$, with phonon wavelength $\lambda = 2\pi c_{T0}'/\omega$. For typical speeds of sound and l in the nanometer range, the corrections to Eq. (3) are small for $\omega \lesssim 10^9$ Hz. This number, 10^9 Hz, is large compared to typical frequencies excited by the probe, since they are expected to be in the range $\omega \sim 10^2 \dots 10^5$ Hz [11, 14, 15, 19, 20, 30–32]. Additionally, Eq. (3) assumes the quality factor $Q(\omega) = \frac{\mu_0}{\omega \eta_0(\omega)}$, the ratio between phonon decay length and phonon wave length, to be large compared to unity. This seems a justified assumption as well, as seen in estimates of the order of $Q \sim 10^4$ [47, 48] (see Table I for experimental parameters). Despite Q being large, phonon attenuation is

essential for friction since, as shown below, it dominates the behavior in certain regimes.

The two leading terms in Eq. (3) have fundamentally different physical origins. The first, called the elastic contribution, corresponds to transport of energy by traveling waves, and it persists without phonon attenuation [16, 42]. The second, called the viscous contribution, is proportional to viscosity η_0 . We discuss its physical origin below. Their relative weight is the dimensionless viscosity,

$$\tilde{\eta} = \frac{\eta_0}{c_{T0}' \rho_0 l} = \frac{\lambda}{2\pi Q l}, \quad (4)$$

which depends on material properties and probe size l . The numbers of Table I for typical AFM conditions imply $\tilde{\eta} \sim 10^5$. We thus first discuss the case of $\tilde{\eta} \gg 1$, where the bulk case of Eq. (3) is dominated by the viscous contribution (using $c_{T0}' = \sqrt{\mu_0/\rho_0} + \mathcal{O}(Q^{-2})$)

$$\lim_{\tilde{\eta} \gg 1} \Gamma^\infty = \frac{\zeta^{\text{vis}} \kappa^2 n_A^2 l^3 \eta_0}{2\mu_0^2}. \quad (5)$$

For finite values of d , we note that the boundary condition at the interface between coating (labeled with the subscript 0) and substrate (subscript 1) is determined by the refractive index $n(\omega) = c_{T0}(\omega)/c_{T1}(\omega)$ and ρ_0/ρ_1 [50]. It is insightful to start with the limit $n = 0$ [51], which yields a Dirichlet boundary condition (DBC) of $\mathbf{u}(\mathbf{r}_{\parallel}, -d, \omega) = \mathbf{0}$ [40, 50]. In this case the substrate is much stiffer than the coating, and phonons are totally reflected at the interface, with phase shift π .

Figure 2 (a) shows Γ as a function of d for $n = 0$ and $\tilde{\eta} \gg 1$, growing linearly in d , and saturating to the bulk value of Eq. (5) for large d , with a cross-over length scale around $d \approx l$. Indeed, we find that, for small d , the leading order of Γ is linear in d ,

$$\Gamma = \frac{\pi \kappa^2 n_A^2 l^2 \eta_0 d}{2\mu_0^2} + \mathcal{O}(d^3) \stackrel{\tilde{\eta} \gg 1}{=} \frac{\pi \Gamma^\infty d}{2\zeta^{\text{vis}} l} + \mathcal{O}(d^3) \quad (\text{DBC}). \quad (6)$$

Γ vanishes as $d \rightarrow 0$, because the coating, when placed on a stiff substrate, supports fewer phonons as $d \rightarrow 0$. In the second step in Eq. (6), we used Eq. (5) to replace Γ^∞ , making apparent the mentioned saturation to Γ^∞ at $d \approx l$. The dependence of Γ on d is *short range*, set by probe size l of Eq. (1).

l ^a	ω ^b	ρ ^c	μ ^c
1 nm	$10^3 \frac{1}{\text{s}}$	$10^{-23} \frac{\text{kg}}{\text{nm}^3}$	$10 \frac{\text{kg}}{\text{nm s}^2}$

^a Refs. [19, 27, 32]. ^b Refs. [19, 20, 30–32]. ^c Ref. [49].

TABLE I. Parameters typical for AFM experiments on solids: radius of contact l , frequency ω , mass density ρ , and shear elastic modulus μ .

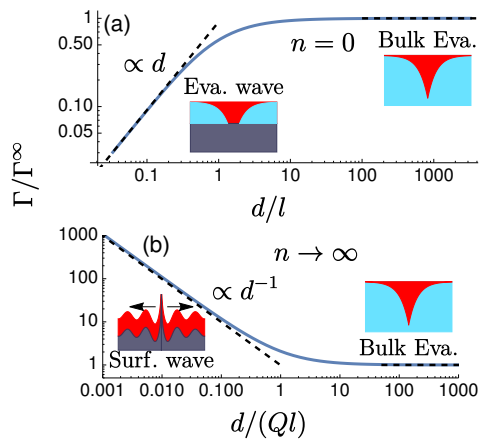


FIG. 2. Damping coefficient Γ for (a) $n = 0$ and (b) $n \rightarrow \infty$ as a function of (scaled) distance d , in the viscous limit $\tilde{\eta} \gg 1$. The solid line shows numerical evaluation, dashed lines give the asymptotes of Eqs. (5), (6) and (7), respectively. Sketches give the fundamental wave solutions in the corresponding regimes.

How is this short range decay possible over distances much smaller than the wavelength? The motion of the probe excites not only (attenuated) traveling waves, but also *evanescent waves* that decay within a range of l . In the presence of finite viscosity, they contribute to energy absorption, and thus to the damping coefficient Γ . In Fig. 2, this mechanism outweighs the energy transported by traveling waves, which is why Eqs. (5) and (6) carry η_0 as a factor.

The opposite limit of boundary conditions, $n \rightarrow \infty$, corresponds to a freestanding coating or a much more compliant substrate, and the waves obey a Neumann BC (NBC), $\hat{e}_z \cdot \boldsymbol{\sigma}(\mathbf{r}_{\parallel}, -d, \omega) = \mathbf{0}$ with stress tensor $\boldsymbol{\sigma}$ and surface normal \hat{e}_z [50]. Phonons are totally reflected without phase shift. This renders Γ fundamentally different from the case of $n = 0$ as shown in Fig. 2 (b); Γ *diverges* for small d and converges to the bulk value on a scale of $d \approx Ql$. Expanding this case for small d yields

$$\Gamma = \frac{11\pi^2\kappa^2 n_A^2 l^4}{64\mu_0|\omega|d} + \mathcal{O}(d) \stackrel{\tilde{\eta} \gg 1}{=} \frac{11\pi^2\Gamma^\infty Ql}{64\zeta^{\text{vis}}d} + \mathcal{O}(d) \quad (\text{NBC}). \quad (7)$$

In this case, the probe excites *traveling surface waves*, $\sim e^{i\omega r_{\parallel}/c_{T0}}/\sqrt{r_{\parallel}}$, i.e., the coating oscillates like a freestanding 2D sheet. Energy is transported along the surface, rather than absorbed; Eq. (7) is independent of viscosity η_0 . As the sheet gets more compliant with $d \rightarrow 0$, amplitudes of excitations get larger, and formally diverge as $d \rightarrow 0$. The second equality of Eq. (7) implies the mentioned saturation length of $d \approx Ql$. With l on the scale of nanometers, this length is of the order of microns. It will be interesting to compare these surface modes to so-called puckering [32, 36] or ploughing [28, 35] identified in previous work.

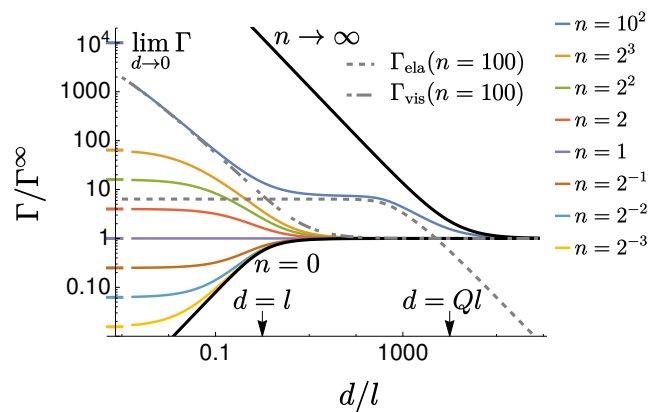


FIG. 3. Damping coefficient Γ for various refractive indices n , using $\tilde{\eta} = 10^5$ and $Q = 10^4$, only considering transverse waves. Marks on the y axis are (analytic) values of $\lim_{d \rightarrow 0} \Gamma$ for the corresponding n . The gray dashed lines are the purely elastic and viscous contributions at $n = 100$.

The cases of $n = 0$ and $n \rightarrow \infty$ provide a reference for the discussion of an arbitrary refractive index n . For simplicity, we assume that the quality factors of the coating and substrate are identical, making $n(\omega)$ real, and use $\rho_0 = \rho_1$ [52]. For finite values of n , we note a numerical challenge in evaluating the longitudinal modes, so that we restrict the shown data to transverse waves (SM).

Figure 3 shows Γ as a function of d for various n , at $\tilde{\eta} = 10^5$ and $Q = 10^4$; Γ is monotonic in d , and stays within the bounds of the limiting cases of $n = 0$ and $n \rightarrow \infty$. Importantly, for a thin coating, $d \rightarrow 0$, Γ approaches the bulk value of the substrate, indicated as bars on the y -axis. These are obtained by Eq. (3) with the material parameters of the substrate [53] [54]. Γ thus varies between the bulk results of the substrate ($d \rightarrow 0$) and of the coating ($d \rightarrow \infty$).

The curves of Fig. 3 up to $n = 2^3$ can be understood by these two limiting cases, and a transition on the length scale l . These cases are thus dominated by evanescent waves. The dimensionless viscosity of the substrate equals $\tilde{\eta}/n$, and goes down for large values of n . The damping coefficient of the bulk substrate, i.e., the behavior at small d , is thus dominated by traveling waves at large n . Indeed, for $n \rightarrow \infty$, the behavior of Fig. 2 (b) is approached. For intermediate values of n ($n = 10^2$ in the graph), a two-step decay occurs, with evanescent waves for $d \lesssim l$ and $d \gtrsim Ql$, and traveling surface waves for $l \lesssim d \lesssim Ql$.

What about the case of $\tilde{\eta} \ll 1$ where the limit $d \rightarrow \infty$ is dominated by traveling waves? Despite less experimental relevance to AFM experiments, we include this insightful case in Fig. 4 for completeness, focusing on $n = 0$ (see SM for $n \rightarrow \infty$). As seen in the Figure, for $d \ll \lambda$ the curves are similar to Fig. 2 (a). This is because, for $n = 0$, the coating *does not support* traveling waves for

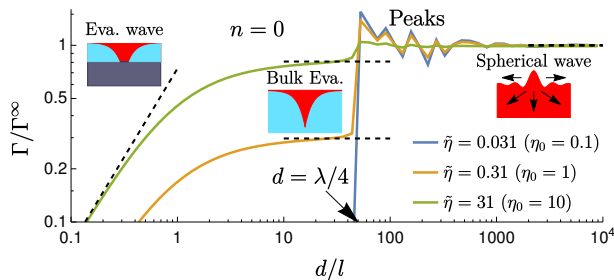


FIG. 4. Damping coefficient Γ as a function of (scaled) distance for $n = 0$, for three values of $\tilde{\eta}$. The black dashed lines represent the asymptotes of Eqs. (3), (5) and (6). For the chosen parameters, the first peak is at $d/l = \lambda/4l \approx 50$.

$d \lesssim \lambda$ (SM). For $d \gtrsim \lambda$, traveling waves are excited, yielding a sharp transition between evanescent and traveling waves at $d \approx \lambda/4$, followed by peaks. These are due to interference effects between outgoing and reflected traveling waves (SM). For $d \gg \lambda$, the bulk value of Eq. (3) is approached.

This discussion allows identification of mechanism regimes, depicted in Fig. 5. The limit of $d \rightarrow \infty$ is dominated by evanescent waves for $\tilde{\eta} \gg 1$, and by traveling waves for $\tilde{\eta} \ll 1$. This is indicated in Fig. 5 by using different colors in the inset graphs. The line $n = \tilde{\eta}$ separates the same for $d \rightarrow 0$, i.e., curves that begin with blue or red. This limit can be found from [55],

$$\lim_{d \rightarrow 0} \Gamma = \Gamma^\infty n^3 \frac{\zeta^{\text{ela}} + \zeta^{\text{vis}} \frac{\tilde{\eta}}{n}}{\zeta^{\text{ela}} + \zeta^{\text{vis}} \tilde{\eta}}. \quad (8)$$

Another separator is $n = 1$, dividing curves where Γ^∞ is larger than the limit of $d \rightarrow 0$ from the opposite. The last curve, $n = \sqrt[3]{\tilde{\eta}}$, together with $n = \tilde{\eta}$, bounds two regimes with multiple transitions between traveling and evanescent waves. The latter occur because of the different d -dependence of traveling and evanescent waves.

This framework identifies the main phononic mechanisms for damping between a probe and a coated planar surface, with vastly different behaviors. These regimes are expected to occur in experiments and simulations, whenever the thickness of coatings can be changed without changing contact mechanics. Fig. 5 illustrates that pronounced dependence on layer thickness is expected, e.g., if the two materials show a refractive index very different from unity. The discussed isolated frequencies apply in non-contact measurements, where narrow frequency bands are excited [11, 13–15]. In sliding experiments, one expects a spectrum of frequencies, so that the results reported here need to be averaged accordingly. It is important to note that the contributions by evanescent waves are frequency independent within the range given below Eq. (3), making this average trivial. Friction from traveling waves has frequency dependent features, see Eq. (7), manifested as the peaks in Fig. 4.

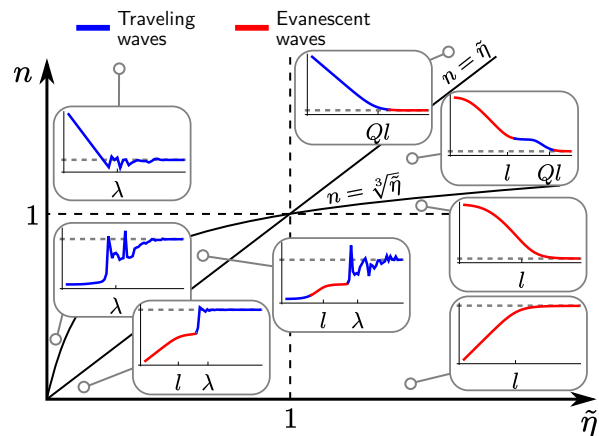


FIG. 5. Friction map. Depending on $\tilde{\eta}$ and n , Γ is dominated by evanescent modes (red) and decays to bulk on a scale $d \approx l$, or by traveling waves (blue), which decay on scales of Ql or λ . The lines separating the regimes are deduced from Eq. (8). Gray dashed lines show the limit $d \rightarrow \infty$ of Eq. (3).

The presented model is simple and provides analytical results, which we expect to improve understanding of friction phenomena. The quantitative translation to the case of sliding motion needs to be investigated in future work [56]. We note however qualitative agreement with studies on graphene. Experiments [32] and simulations [27] reported friction on freely standing graphene flakes, i.e., $n \gg 1$, finding a decrease with increasing number of layers. The same trend is observed for mounted graphene layers (or flakes) [27, 30–32]; graphene is much stiffer ($\mu \sim 1$ TPa [45, 57, 58]) than metal substrates ($\mu \sim 10$ GPa [49, 59]), so that the case of $n \gg 1$ applies too. Previous work attributed this behavior to the enhanced rigidity for thicker samples [27, 32], leading to the suppression of surface waves, in agreement with our findings.

The framework of Eq. (2) naturally includes Hertzian contact theory [40, 60] in the limit of small frequencies. It is interesting to remark that the identified evanescent waves can equally be found from the slowly moving distortion field of contact theory. Moving this distortion field dissipates energy due to viscosity (SM). This way, this approach can be linked to a variety of other approaches based on contact theory [4, 7, 18, 56] and local deformations [28, 29, 36]. Natural extensions include nonlinear systems, where, e.g., deeper indentations [28, 29, 36] can be studied. Lateral confinement was also found to be of importance [8], and it provides an interesting additional possibility to identify involved phonon modes. This can be address in the presented framework in future work.

This work was funded by the Deutsche Forschungsgemeinschaft (DFG, German Research Foundation) - 217133147 via SFB 1073 (Project A01). We thank Richard L.C. Vink for stimulating discussions. In mem-

ory of Philip Rauch.

* miru.lee@uni-goettingen.de

† matthias.kruger@uni-goettingen.de

- [1] L. Prandtl, *Zeitschrift für Angewandte Mathematik und Mechanik* **8**, 85 (1928).
- [2] M. H. Müser, *Physical Review B* **84**, 125419 (2011).
- [3] B. N. Persson, *Sliding friction: physical principles and applications* (Springer Science & Business Media, 2013).
- [4] B. N. Persson, O. Albohr, F. Mancosu, V. Peveri, V. Samoilov, and I. M. Sivebæk, *Wear* **254**, 835 (2003).
- [5] E. Gnecco, R. Bennewitz, T. Gyalog, C. Loppacher, M. Bammmerlin, E. Meyer, and H.-J. Güntherodt, *Physical Review Letters* **84**, 1172 (2000).
- [6] A. Socoliuc, R. Bennewitz, E. Gnecco, and E. Meyer, *Physical Review Letters* **92**, 134301 (2004).
- [7] C. Qu, K. Wang, J. Wang, Y. Gongyang, R. W. Carpick, M. Urbakh, and Q. Zheng, *Physical Review Letters* **125**, 126102 (2020).
- [8] N. Wada, M. Ishikawa, T. Shiga, J. Shiomi, M. Suzuki, and K. Miura, *Physical Review B* **97**, 161403 (2018).
- [9] I. A. Boldin, A. Kraft, and C. Wunderlich, *Physical Review Letters* **120**, 023201 (2018).
- [10] A. I. Volokitin and B. N. J. Persson, *Physical Review B* **63**, 205404 (2001).
- [11] I. Dorofeyev, H. Fuchs, G. Wenning, and B. Gotsmann, *Physical Review Letters* **83**, 2402 (1999).
- [12] A. I. Volokitin and B. N. J. Persson, *Reviews of Modern Physics* **79**, 1291 (2007).
- [13] M. Kisiel, E. Gnecco, U. Gysin, L. Marot, S. Rast, and E. Meyer, *Nature Materials* **10**, 119 (2011).
- [14] B. C. Stipe, H. J. Mamin, T. D. Stowe, T. W. Kenny, and D. Rugar, *Physical Review Letters* **87**, 096801 (2001).
- [15] B. Gotsmann and H. Fuchs, *Physical Review Letters* **86**, 2597 (2001).
- [16] B. N. J. Persson and R. Ryberg, *Physical Review B* **32**, 3586 (1985).
- [17] A. I. Volokitin, B. N. J. Persson, and H. Ueba, *Physical Review B* **73**, 165423 (2006).
- [18] R. Hu, S. Y. Krylov, and J. W. Frenken, *Tribology Letters* **68**, 1 (2020).
- [19] N. A. Weber, H. Schmidt, T. Sievert, C. Jooss, F. Güthoff, V. Moshneaga, K. Samwer, M. Krüger, and C. A. Volkert, *Advanced Science* **8**, 2003524 (2021).
- [20] H. Schmidt, J.-O. Krisponeit, N. Weber, K. Samwer, and C. A. Volkert, *Physical Review Materials* **4**, 113610 (2020).
- [21] L. Kantorovich, *Physical Review B* **78**, 094304 (2008).
- [22] L. Kantorovich and N. Rompotis, *Physical Review B* **78**, 094305 (2008).
- [23] E. Panizon, G. E. Santoro, E. Tosatti, G. Riva, and N. Manini, *Physical Review B* **97**, 104104 (2018).
- [24] C. Daly and J. Krim, *Physical Review Letters* **76**, 803 (1996).
- [25] S. Kajita, H. Washizu, and T. Ohmori, *Europhysics Letters* **87**, 66002 (2009).
- [26] L. Xu, T.-B. Ma, Y.-Z. Hu, and H. Wang, *Nanotechnology* **22**, 285708 (2011).
- [27] A. Smolyanitsky, J. P. Killgore, and V. K. Tewary, *Physical Review B* **85**, 035412 (2012).
- [28] A. Smolyanitsky and J. P. Killgore, *Physical Review B* **86**, 125432 (2012).
- [29] A. Smolyanitsky, *Rsc Advances* **5**, 29179 (2015).
- [30] T. Filleter, J. L. McChesney, A. Bostwick, E. Rotenberg, K. V. Emtsev, T. Seyller, K. Horn, and R. Bennewitz, *Physical Review Letters* **102**, 086102 (2009).
- [31] T. Filleter and R. Bennewitz, *Physical Review B* **81**, 155412 (2010).
- [32] C. Lee, Q. Li, W. Kalb, X.-Z. Liu, H. Berger, R. W. Carpick, and J. Hone, *Science* **328**, 76 (2010).
- [33] D. Berman, A. Erdemir, and A. V. Sumant, *Materials Today* **17**, 31 (2014).
- [34] A. Benassi, A. Vanossi, G. E. Santoro, and E. Tosatti, *Physical Review B* **82**, 081401(R) (2010).
- [35] Z. Deng, A. Smolyanitsky, Q. Li, X.-Q. Feng, and R. J. Cannara, *Nature materials* **11**, 1032 (2012).
- [36] S. Li, Q. Li, R. W. Carpick, P. Gumbsch, X. Z. Liu, X. Ding, J. Sun, and J. Li, *Nature* **539**, 541 (2016).
- [37] H. Risken, *The Fokker-Planck Equation* (Springer, Berlin, 1996).
- [38] H. C. Hamaker, *Physica* **4**, 1058 (1937).
- [39] W. N. Findley, J. S. Lai, and K. Onaran, *Creep and Relaxation of Nonlinear Viscoelastic Materials, with an Introduction to Linear Viscoelasticity* (North-Holland Publishing Company, New York, N.Y., 2013).
- [40] L. Landau, E. Lifshitz, J. Sykes, and W. Reid, *Theory of elasticity: Volume 7 of course of theoretical physics*, Vol. 7 (Elsevier, Oxford, 1986).
- [41] E. Lee, *Quarterly of Applied Mathematics* **13**, 183 (1955).
- [42] M. Lee, R. L. C. Vink, C. A. Volkert, and M. Krüger, *Physical Review B* **104**, 174309 (2021).
- [43] W. Gornall and B. Stoicheff, *Physical Review B* **4**, 4518 (1971).
- [44] H. Petert, J. Skalyo Jr, H. Grimm, E. Lüscher, and P. Korpiun, *Journal of Physics and Chemistry of Solids* **34**, 255 (1973).
- [45] X. Cong, Q.-Q. Li, X. Zhang, M.-L. Lin, J.-B. Wu, X.-L. Liu, P. Venezuela, and P.-H. Tan, *Carbon* **149**, 19 (2019).
- [46] B. N. J. Persson, E. Tosatti, D. Fuhrmann, G. Witte, and C. Wöll, *Physical Review B* **59**, 11777 (1999).
- [47] K. Ono, *Applied Sciences* **10**, 2230 (2020).
- [48] B. N. Persson, *The Journal of Chemical Physics* **115**, 3840 (2001).
- [49] B. A. Auld, *Acoustic fields and waves in solids* (John Wiley & Sons Inc., 1973).
- [50] L. M. Brekhovskikh, *Waves in layered media* (Academic Press, New York, 1980).
- [51] For $n = 0$, ρ_0/ρ_1 is irrelevant.
- [52] These two assumptions can be relaxed without additional challenge, yielding similar conclusions as the ones presented.
- [53] We assume that the surface coupling (here κ , n_A and l) are the same for coating and for pure substrate.
- [54] In experiments, the limit $d \rightarrow 0$ (thin coating) is expected to be different from $d = 0$ (no coating), because of different surface interactions for substrate and coating.
- [55] See the SM for more discussion and the general case where n is complex and $\rho_0 \neq \rho_1$.
- [56] N. A. Weber, M. Lee, F. Schönewald, L. Schüler, V. Moshnyaga, M. Krüger, and C. A. Volkert, arXiv preprint arXiv:2210.09677 (2022).
- [57] J.-U. Lee, D. Yoon, and H. Cheong, *Nano letters* **12**, 4444 (2012).

- [58] G. Van Lier, C. Van Alsenoy, V. Van Doren, and P. Geerlings, *Chemical Physics Letters* **326**, 181 (2000).
- [59] J.-H. Zhao, T. Ryan, P. S. Ho, A. J. McKerrow, and W.-Y. Shih, *Journal of Applied Physics* **85**, 6421 (1999).
- [60] K. L. Johnson, *Proceedings of the Institution of Mechanical Engineers* **196**, 363 (1982).

Supplementary Material

Miru Lee,^{1,*} Niklas Weber,² Cynthia A. Volkert,² and Matthias Krüger^{1,†}

¹*Institute for Theoretical Physics, Georg-August-Universität Göttingen, 37073 Göttingen, Germany*

²*Institute of Materials Physics, Georg-August-Universität Göttingen, 37073 Göttingen, Germany*

(Dated: May 24, 2023)

DAMPING COEFFICIENT

The damping coefficient can be calculated from a Green-Kubo relation [1–4],

$$\Gamma = \frac{1}{2k_{\text{B}}T} \int_{-\infty}^{\infty} \frac{d\omega'}{2\pi} \langle F(X, \omega); F(X, \omega') \rangle, \quad (1)$$

where $\langle A; B \rangle = \langle (A - \langle A \rangle)(B - \langle B \rangle) \rangle$ is an ensemble average of the covariance. With the force defined in [Eq. (1)] in the main text, the damping coefficient can be rewritten as

$$\begin{aligned} \Gamma &= \frac{\kappa^2 n_A^2}{2k_{\text{B}}T} \int_{-\infty}^{\infty} d^2 \mathbf{r}_{\parallel} \int_{-\infty}^{\infty} d^2 \mathbf{r}'_{\parallel} \int_{-\infty}^{\infty} \frac{d\omega'}{2\pi} e^{-\frac{r_{\parallel}^2}{t^2}} \langle u_x(\mathbf{r}_{\parallel}, \omega) u_x(\mathbf{r}'_{\parallel}, \omega') \rangle e^{-\frac{r'_{\parallel}{}^2}{t^2}} \\ &= \frac{\kappa^2 n_A^2}{\omega} \int_{-\infty}^{\infty} d^2 \mathbf{r}_{\parallel} \int_{-\infty}^{\infty} d^2 \mathbf{r}'_{\parallel} e^{-\frac{r_{\parallel}^2}{t^2}} \text{Im} \{ G(\mathbf{r}_{\parallel}, \mathbf{r}'_{\parallel}, \omega) \} e^{-\frac{r'_{\parallel}{}^2}{t^2}} \\ &= \frac{\kappa^2 n_A^2}{\omega} \text{Im} \left\{ \int_{-\infty}^{\infty} d^2 \mathbf{r}_{\parallel} \int_{-\infty}^{\infty} d^2 \mathbf{r}'_{\parallel} e^{-\frac{r_{\parallel}^2}{t^2}} G(\mathbf{r}_{\parallel}, \mathbf{r}'_{\parallel}, \omega) e^{-\frac{r'_{\parallel}{}^2}{t^2}} \right\} \end{aligned} \quad (2)$$

Note that in the second equality, we make use of the FDT [4–9],

$$\int_{-\infty}^{\infty} \frac{d\omega'}{2\pi} \langle u_x(\mathbf{r}, \omega) u_x(\mathbf{r}', \omega') \rangle = \frac{2k_{\text{B}}T}{\omega} \text{Im} \{ G(\mathbf{r}, \mathbf{r}', \omega) \}. \quad (3)$$

It is more convenient to obtain the Green's function in $\mathbf{k}_{\parallel} = (k_x, k_y)$ space, since the Kelvin-Voigt model ([Eq. (2)] in the main text) becomes an ordinary differential equation. Let us change the spatial integral to an integral over \mathbf{k}_{\parallel} space,

$$\begin{aligned} \Gamma &= \frac{\kappa^2 n_A^2}{\omega} \text{Im} \left\{ \int_{-\infty}^{\infty} d^2 \mathbf{r}_{\parallel} \int_{-\infty}^{\infty} d^2 \mathbf{r}'_{\parallel} e^{-\frac{r_{\parallel}^2}{t^2}} G(\mathbf{r}_{\parallel}, \mathbf{r}'_{\parallel}, \omega) e^{-\frac{r'_{\parallel}{}^2}{t^2}} \right\} \\ &= \frac{\kappa^2 n_A^2}{\omega} \text{Im} \left\{ \int d^2 \mathbf{r}_{\parallel} \int d^2 \mathbf{r}'_{\parallel} \int_{-\infty}^{\infty} \frac{d^2 \mathbf{k}_{\parallel}}{(2\pi)^2} \int_{-\infty}^{\infty} \frac{d^2 \mathbf{k}'_{\parallel}}{(2\pi)^2} e^{-\frac{r_{\parallel}^2}{t^2}} G(\mathbf{k}_{\parallel}, z=0, \mathbf{k}'_{\parallel}, z'=0, \omega) e^{-\frac{r'_{\parallel}{}^2}{t^2}} e^{i\mathbf{k}_{\parallel} \cdot \mathbf{r}_{\parallel}} e^{i\mathbf{k}'_{\parallel} \cdot \mathbf{r}'_{\parallel}} \right\} \\ &= \frac{\kappa^2 n_A^2 l^4 \pi^2}{\omega} \text{Im} \left\{ \int_{-\infty}^{\infty} \frac{d^2 \mathbf{k}_{\parallel}}{(2\pi)^2} \int_{-\infty}^{\infty} \frac{d^2 \mathbf{k}'_{\parallel}}{(2\pi)^2} e^{-\frac{k_{\parallel}^2 t^2}{4}} G(\mathbf{k}_{\parallel}, 0, \mathbf{k}'_{\parallel}, 0, \omega) e^{-\frac{k'_{\parallel}{}^2 t^2}{4}} \right\}. \end{aligned} \quad (4)$$

The above expression for the damping coefficient can be further simplified if the homogeneity of the Green's function is assumed, i.e., $G(\mathbf{r} + \mathbf{r}_0, \mathbf{r}' + \mathbf{r}_0, \omega) = G(\mathbf{r}, \mathbf{r}', \omega)$ [10],

$$\begin{aligned} G(\mathbf{k}, \mathbf{k}', \omega) &= \int_{-\infty}^{\infty} d^3 \mathbf{r} \int_{-\infty}^{\infty} d^3 \mathbf{r}' G(\mathbf{r} + \mathbf{r}_0, \mathbf{r}' + \mathbf{r}_0, \omega) e^{-i\mathbf{k} \cdot (\mathbf{r} + \mathbf{r}_0)} e^{-i\mathbf{k}' \cdot (\mathbf{r}' + \mathbf{r}_0)} \\ &= \int_{-\infty}^{\infty} d^3 \mathbf{r} \int_{-\infty}^{\infty} d^3 \mathbf{r}' G(\mathbf{r}, \mathbf{r}', \omega) e^{-i\mathbf{k} \cdot \mathbf{r}} e^{-i\mathbf{k}' \cdot \mathbf{r}'} e^{-i\mathbf{r}_0 \cdot (\mathbf{k} + \mathbf{k}')} \\ &= G(\mathbf{k}, \mathbf{k}', \omega) e^{-i\mathbf{r}_0 \cdot (\mathbf{k} + \mathbf{k}')}. \end{aligned} \quad (5)$$

The homogeneity thus entails $\mathbf{k} = -\mathbf{k}'$, i.e.,

$$G(\mathbf{k}, \mathbf{k}', \omega) = (2\pi)^3 G(\mathbf{k}, \omega) \delta(\mathbf{k} + \mathbf{k}'). \quad (6)$$

Or,

$$G(\mathbf{k}_{\parallel}, z, \mathbf{k}'_{\parallel}, z', \omega) = (2\pi)^2 G(\mathbf{k}_{\parallel}, z - z', \omega) \delta(\mathbf{k}_{\parallel} + \mathbf{k}'_{\parallel}). \quad (7)$$

Plugging it into Eq. (4), one arrives at

$$\Gamma = \frac{\kappa^2 n_A^2 l^4 \pi^2}{\omega} \text{Im} \left\{ \int_{-\infty}^{\infty} \frac{d^2 \mathbf{k}_{\parallel}}{(2\pi)^2} G(\mathbf{k}_{\parallel}, 0, \omega) e^{-\frac{1}{2} k_{\parallel}^2 l^2} \right\}, \quad (8)$$

which we use to evaluate the damping coefficient both numerically and analytically.

BOUNDARY CONDITIONS

Regarding the geometry of the system, it has the surface at $z = 0$ in the xy plane, while extending infinitely in the x and y directions. For $z > 0$, it is a vacuum, i.e., no phonon can exist. The boundary conditions (BC) at $z = 0$ are given by [11–14]

$$\sigma_{xz}(\mathbf{r}_{\parallel}, \omega) = \kappa X(\omega) e^{-\frac{r_{\parallel}^2}{l^2}}, \quad (9)$$

while other components are zero. Here, $\boldsymbol{\sigma}(\mathbf{r}, \omega)$ is the Cauchy stress tensor, which is defined as

$$\boldsymbol{\sigma} = \rho(c_L^2 - 2c_T^2) \nabla \cdot \mathbf{u} + \rho c_T^2 (\nabla \mathbf{u} + (\nabla \mathbf{u})^T). \quad (10)$$

Note that the BC on the surface suggest that the displacement field $u_x(\mathbf{r}, \omega)$ is linearly proportional to the position of the probe $X(\omega)$, containing the phase information with respect to $X(\omega)$, which, in turn, yields a finite damping coefficient.

For $-d < z \leq 0$, we have the first layer (the coating) of the solid whose properties are characterized by $c_{L0}(\omega)$, $c_{T0}(\omega)$, and ρ_0 . The second layer (the substrate) expands for $-\infty < z < -d$ with $c_{L1}(\omega)$, $c_{T1}(\omega)$, and ρ_1 . The BC at $z = -d$ require that the displacement field and traction are continuous [15],

$$\begin{aligned} \lim_{z \rightarrow -d^+} \mathbf{u}(\mathbf{r}, \omega) &= \lim_{z \rightarrow -d^-} \mathbf{u}(\mathbf{r}, \omega), \\ \lim_{z \rightarrow -d^+} \hat{\mathbf{e}}_z \cdot \boldsymbol{\sigma}(\mathbf{r}, \omega) &= \lim_{z \rightarrow -d^-} \hat{\mathbf{e}}_z \cdot \boldsymbol{\sigma}(\mathbf{r}, \omega), \end{aligned} \quad (11)$$

where $\hat{\mathbf{e}}_z$ is the unit vector in the z direction. The Dirichlet and Neumann BC in the main text are the special cases of the above BC.

TRAVELING VS. EVANESCENT WAVE

Here, we show that traveling waves yield the elastic contribution, and evanescent waves the viscous contribution. Since any wave can be expressed by a superposition of plane waves, an ansatz of the transverse motion of the solid ([Eq. (2)] in the main text) can be written as

$$G_T(\mathbf{k}_{\parallel}, z - z', d, \omega) = C_0(\mathbf{k}_{\parallel}, d, \omega) e^{q_T(z-z')} + C_1(\mathbf{k}_{\parallel}, d, \omega) e^{-q_T(z-z')}, \quad (12)$$

where $q_T = (k_{\parallel}^2 - \omega^2/c_T^2)^{1/2}$, and $C_0(\mathbf{k}_{\parallel}, d, \omega)$ ($C_1(\mathbf{k}_{\parallel}, d, \omega)$) is an amplitude of outgoing (incoming) wave. The longitudinal counterpart can be similarly written with $q_L = (k_{\parallel}^2 - \omega^2/c_L^2)^{1/2}$, which then gives us the full solution $G = G_T + G_L$. From the ansatz, it follows that if $k_{\parallel} \leq \omega/c_T$, the solution represents a traveling wave in the z direction. Contrarily, if $k_{\parallel} \geq \omega/c_T$, then it decays exponentially in the z coordinate, i.e., an evanescent wave, resulting from an adiabatic deformation (see below).

Notice also that the integral in Eq. (8) runs in \mathbf{k}_{\parallel} space, along which there may exist branches or singularities. Consequently, the integral can be divided into many parts according to the branch or/and singular points,

$$\begin{aligned} \Gamma &= \frac{\kappa^2 n_A^2 l^4}{4\omega} \text{Im} \left\{ \int_0^{2\pi} d\theta \left[\int_0^{k_{s,1}} dk_{\parallel} k_{\parallel} G(\mathbf{k}_{\parallel}, 0, d, \omega) e^{-\frac{1}{2} k_{\parallel}^2 l^2} + \int_{k_{s,1}}^{k_{s,2}} dk_{\parallel} k_{\parallel} G(\mathbf{k}_{\parallel}, 0, d, \omega) e^{-\frac{1}{2} k_{\parallel}^2 l^2} \right. \right. \\ &\quad \left. \left. + \int_{k_{s,2}}^{k_{s,3}} dk_{\parallel} k_{\parallel} G(\mathbf{k}_{\parallel}, 0, d, \omega) e^{-\frac{1}{2} k_{\parallel}^2 l^2} + \dots + \int_{k_{s,N}}^{\infty} dk_{\parallel} k_{\parallel} G(\mathbf{k}_{\parallel}, 0, d, \omega) e^{-\frac{1}{2} k_{\parallel}^2 l^2} \right] \right\} \end{aligned} \quad (13)$$

where $k_{s,n}$ $n \in \{1, 2, \dots, N\}$ are the branch and singular points of the Green's function. In what follows, we show that the terms running up to $k_{s,N}$ integrate traveling waves resulting in the elastic contribution, and the last term evanescent waves resulting in the viscous contribution.

Let us exemplarily consider the transverse mode. The Green's function at $z = z'$ (the argument is henceforth omitted) at the limit of $d \gg \lambda$ reads,

$$G_{\text{T}}(\mathbf{k}_{\parallel}, \omega) = \frac{\sin^2 \theta}{\rho_0 c_{\text{T}0}^2 q_{\text{T}0}}. \quad (14)$$

The branch point is located at $k_s = \omega/c_{\text{T}0}$. Note that this branch point coincides with the singularity. The integration is thus divided into two parts. The first part integrates traveling waves,

$$\frac{\kappa^2 n_{\text{A}}^2 l^4}{4\omega} \int_0^{2\pi} d\theta \int_0^{\omega/c_{\text{T}0}} dk_{\parallel} k_{\parallel} \frac{\sin^2 \theta}{\rho_0 c_{\text{T}0}^2 q_{\text{T}0}} e^{-\frac{1}{2} k_{\parallel}^2 l^2} = -\frac{\pi^{3/2} \kappa^2 n_{\text{A}}^2 l^3 e^{-l^2 \omega^2 / (2c_{\text{T}0}^2)}}{2^{5/2} c_{\text{T}0}^2 \rho_0 \omega} \operatorname{erf}\left(\frac{-il\omega}{\sqrt{2}c_{\text{T}0}}\right), \quad (15)$$

where $\operatorname{erf}(x)$ is the error function. Expanding it at a small ω and taking the imaginary part, one arrives at

$$\operatorname{Im} \left\{ -\frac{\pi^{3/2} \kappa^2 n_{\text{A}}^2 l^3 e^{-l^2 \omega^2 / (2c_{\text{T}0}^2)}}{2^{5/2} c_{\text{T}0}^2 \rho_0 \omega} \operatorname{erf}\left(\frac{-il\omega}{\sqrt{2}c_{\text{T}0}}\right) \right\} = \frac{\pi \kappa^2 n_{\text{A}}^2 l^4}{4} \sqrt{\frac{\rho_0}{\mu_0^3}} + \mathcal{O}\left(\frac{1}{Q^2}, \frac{l^2}{\lambda^2}\right). \quad (16)$$

Note that one should perform the integral first and then the expansion, since the singularity renders these operations non-commute. Note also that the leading order of this contribution is *independent* of viscosity η_0 .

The second part, on the contrary, takes care of the evanescent wave solution

$$\begin{aligned} & \frac{\kappa^2 n_{\text{A}}^2 l^4}{4\omega} \int_0^{2\pi} d\theta \int_{\omega/c_{\text{T}0}}^{\infty} dk_{\parallel} k_{\parallel} \frac{\sin^2 \theta}{\rho_0 c_{\text{T}0}^2 q_{\text{T}0}} e^{-\frac{1}{2} k_{\parallel}^2 l^2} \\ &= \frac{\pi \kappa^2 n_{\text{A}}^2 l^4}{4\omega} \int_0^{2\pi} d\theta \int_0^{\infty} dk_{\parallel} k_{\parallel} \sin^2 \theta \left[\frac{1}{k_{\parallel} \mu_0} + \frac{i\omega \eta_0}{k_{\parallel} \mu_0^2} \right] e^{-\frac{1}{2} k_{\parallel}^2 l^2} + \mathcal{O}\left(\frac{1}{Q^2}\right). \end{aligned} \quad (17)$$

Here, we expanded the integrand for small ω first, since the integral over k_{\parallel} and the limit of $\omega \rightarrow 0$ commute [4]. Performing the integration leads us to

$$\frac{\pi \kappa^2 n_{\text{A}}^2 l^4}{4\omega} \int_0^{2\pi} d\theta \int_0^{\infty} dk_{\parallel} k_{\parallel} \sin^2 \theta \left[\frac{1}{k_{\parallel} \mu_0} + \frac{i\omega \eta_0}{k_{\parallel} \mu_0^2} \right] e^{-\frac{1}{2} k_{\parallel}^2 l^2} = \frac{\pi^{3/2} \kappa^2 n_{\text{A}}^2 l^3}{2^{5/2} \omega} \left[\frac{1}{\mu_0} + \frac{i\omega \eta_0}{\mu_0^2} \right]. \quad (18)$$

Taking the imaginary part, one finds the friction contribution from evanescent waves

$$\frac{\pi^{3/2} \kappa^2 n_{\text{A}}^2 l^3 \eta_0}{2^{5/2} \mu_0^2} + \mathcal{O}\left(\frac{1}{Q^2}\right). \quad (19)$$

Unlike the elastic contribution from traveling waves, the leading order is linearly proportional to the viscosity η_0 . Putting them together, we find

$$\begin{aligned} \Gamma_{\text{T}}^{\infty} &= \frac{\pi \kappa^2 n_{\text{A}}^2 l^4}{4} \sqrt{\frac{\rho_0}{\mu_0^3}} + \frac{\pi^{3/2} \kappa^2 n_{\text{A}}^2 l^3 \eta_0}{2^{5/2} \mu_0^2} + \mathcal{O}\left(\frac{1}{Q^2}, \frac{l^2}{\lambda^2}\right) \\ &= \frac{\pi \kappa^2 n_{\text{A}}^2 l^4}{4 \rho c_{\text{T}0}^3} \left(1 + \sqrt{\frac{\pi}{2}} \frac{\eta_0}{\rho_0 c_{\text{T}0} l} \right) + \mathcal{O}\left(\frac{1}{Q^2}, \frac{l^2}{\lambda^2}\right). \end{aligned} \quad (20)$$

It is noteworthy that the existence of a branch point or a singularity at a finite value of k_{\parallel} directly indicates the existence of a traveling wave. If the Green's function exhibits no such point, then the corresponding wave is purely evanescent.

EVANESCENT WAVES AND LOCAL DEFORMATION

In this section, we show that evanescent waves represent the adiabatic local deformation due to the probe-sample interaction F , i.e., the Hertzian contact. The adiabatic local deformation can be obtained when the inertial term

in [Eq. (2)] in the main text vanishes [11, 13, 14]. Exemplarily, let us consider the semi-infinite solid. The Green's function for the transverse mode reads

$$G_T(k_{\parallel}) = \sin^2 \theta \left[\frac{1}{k_{\parallel} \mu_0} + \frac{i\omega \eta_0}{k_{\parallel} \mu_0^2} \right]. \quad (21)$$

This expression is precisely the Green's function in the rhs of Eq. (17). Note that since the probe-sample interaction acts parallel to the surface, this deformation represents the local shearing (e.g., puckering). Importantly, the local deformation contributes to the friction if and only if the solid is *viscoelastic*. This is because it is the imaginary part of the Green's function that gives rise to the damping coefficient, which is non-zero only for viscoelastic solids.

FUNDAMENTAL SOLUTIONS

For the Dirichlet BC, the Green's function at the surface ($z = z' = 0$), for d being the smallest length scale, is given by

$$G(\mathbf{k}_{\parallel}, d, \omega) = \frac{d}{c_{T0}^2 \rho_0} + \mathcal{O}(d^3). \quad (22)$$

The leading order has no branch or singular point, meaning that it is evanescent. Since it is constant in \mathbf{k}_{\parallel} space, the above expression becomes a delta function in \mathbf{r}_{\parallel} space,

$$G(\mathbf{r}_{\parallel} - \mathbf{r}'_{\parallel}, d, \omega) = \frac{d}{c_{T0}^2 \rho_0} \delta^{(2)}(\mathbf{r}_{\parallel} - \mathbf{r}'_{\parallel}) + \mathcal{O}(d^3). \quad (23)$$

For the Neumann BC, the Green's function reads

$$G(\mathbf{k}_{\parallel}, d, \omega) = \frac{c_{L0}^2 (k_{\parallel}^2 - q_{L0}^2) (k_y^2 + q_{T0}^2) - 2c_{T0}^2 k_y^2 (k_{\parallel}^2 - 2q_{L0}^2 + q_{T0}^2)}{dc_{T0}^2 \rho_0 q_{T0}^2 (c_{L0}^2 (k_{\parallel}^2 - q_{L0}^2) (k_{\parallel}^2 + q_{T0}^2) - 2c_{T0}^2 k_{\parallel}^2 (k_{\parallel}^2 - 2q_{L0}^2 + q_{T0}^2))} + \mathcal{O}(d). \quad (24)$$

One can easily tell it can be either a traveling or evanescent wave due to the existence of the singular point. By finding the real space counterpart, one can easily identify the dimensional nature of the solution. Assuming $c_{T0} = \sqrt{3}c_{L0}$, it is

$$G(\mathbf{r}_{\parallel} - \mathbf{r}'_{\parallel}, d, \omega) = \frac{8(y - y')^2 K_0 \left(-\frac{i|\mathbf{r}_{\parallel} - \mathbf{r}'_{\parallel}| \omega}{c_{T0}} \right) + 3(x - x')^2 K_0 \left(-\frac{i\sqrt{3}|\mathbf{r}_{\parallel} - \mathbf{r}'_{\parallel}| \omega}{2\sqrt{2}c_{T0}} \right)}{16\pi \rho_0 c_{T0}^2 |\mathbf{r}_{\parallel} - \mathbf{r}'_{\parallel}|^2 d} + \mathcal{O}(d), \quad (25)$$

where K_0 is the Bessel function of the second kind of the zeroth order, a form of surface (2D) waves.

At a large $d \gg \lambda$ on the other hand, the Green's function is given by

$$G(\mathbf{k}_{\parallel}, \omega) = \frac{c_{L0}^2 (k_{\parallel}^2 - q_{L0}^2) (k_y^2 + q_{T0}^2) - 2c_{T0}^2 k_y^2 (k_{\parallel}^2 - 2q_{L0} q_{T0} + q_{T0}^2)}{c_{T0}^2 \rho_0 q_{T0} (c_{L0}^2 (k_{\parallel}^2 - q_{L0}^2) (k_{\parallel}^2 + q_{T0}^2) - 2c_{T0}^2 k_{\parallel}^2 (k_{\parallel}^2 - 2q_{L0} q_{T0} + q_{T0}^2))}. \quad (26)$$

This, again, can be either a traveling or evanescent wave, however, finding the exact expression of the real space counterpart seems difficult. A simpler way to see the dimensionality of the fundamental solution is to only consider the transverse mode, i.e., Eq. (14). In real space, it is given by

$$G_T(\mathbf{r}_{\parallel} - \mathbf{r}'_{\parallel}, \omega) = -\frac{(y - y')^2 e^{\frac{i|\mathbf{r}_{\parallel} - \mathbf{r}'_{\parallel}| \omega}{c_{T0}}}}{2\pi \rho_0 c_{T0}^2 |\mathbf{r}_{\parallel} - \mathbf{r}'_{\parallel}|^3}, \quad (27)$$

which is a spherical (3D) wave solution.

Upon arriving at these fundamental wave solutions, no assumption on $\tilde{\eta}$ is made. In fact, $\tilde{\eta}$ can only be defined after obtaining Eq. (26). This means, mathematically, that [Eqs. (6) and (7)] in the main text are valid for all $\tilde{\eta}$.

THE DAMPING COEFFICIENT FOR AN ARBITRARY INTERACTION AT THE LIMITING CASES

Let us consider a general way to formulate the probe-sample interaction F . Such an interaction arises from the underlying pairwise probe-atom interaction $g(\mathbf{X}, \mathbf{r}_{\parallel}, \omega)$ (it can easily be generalized for vectors as well),

$$F(X, \omega) = n_A \int_{-\infty}^{\infty} d^2 \mathbf{r}_{\parallel} g(X, \mathbf{r}_{\parallel}, \omega). \quad (28)$$

Expanding the pairwise interaction in u_x , one finds

$$g(X, \mathbf{r}_{\parallel}, \omega) = g(X, \mathbf{r}_{\parallel}) + \frac{\partial}{\partial x} g(X, \mathbf{r}_{\parallel}) \cdot u_x(\mathbf{r}_{\parallel}, \omega) + \dots \quad (29)$$

If $\sqrt{\langle u_x^2(\mathbf{r}_{\parallel}, \omega) \rangle} \ll |\mathbf{r}_{\parallel} - X|$ is assumed, the first term can be seen as the pairwise interaction in phase with the motion of X , and the second term out of phase. Now one can calculate the damping coefficient similarly as Eq. (2).

Let us consider the case of small d . For the Dirichlet BC, we use Eq. (22) for the Green's function and perform the integral. Because the Green's function is independent of \mathbf{k}_{\parallel} for the leading order of d , the damping coefficient is given simply by the integration of the interaction,

$$\Gamma = \frac{n_A^2 \eta_0 d}{\mu_0^2} \int_{-\infty}^{\infty} \frac{d^2 \mathbf{k}_{\parallel}}{(2\pi)^2} \left| \frac{\partial}{\partial x} g(X, \mathbf{k}_{\parallel}) \right|^2. \quad (30)$$

The linear dependence of the damping coefficient on the coating thickness d is thus universal to any type of interaction.

For the Neumann BC, the Green's function is given by Eq. (24), which, for $c_{T0} = \sqrt{3}c_{L0}$, reduces to

$$G'(k_{\parallel}, \omega) = \int_0^{2\pi} d\theta G(\mathbf{k}_{\parallel}, \omega) = \frac{\pi(11c_{T0}^2 k_{\parallel}^2 - 6\omega^2)}{d\rho_0(c_{T0}^2 k_{\parallel}^2 - \omega^2)(8c_{T0}^2 k_{\parallel}^2 - 3\omega^2)}. \quad (31)$$

Note that $g(X, \mathbf{k}_{\parallel})$ is azimuthally symmetric, so that it can be factored out of the integral over θ . The integral over k_{\parallel} can be done by means of the residue theorem due to the singularities at

$$k_{\parallel} = \frac{\omega}{c_{T0}(\omega)}, \quad k_{\parallel} = \sqrt{\frac{3}{8}} \frac{\omega}{c_{T0}(\omega)}, \quad (32)$$

yielding the elastic contribution from traveling waves. The remaining integrals that are associated with the residue theorem contributes to higher order terms in ω (i.e., $\mathcal{O}(d/\lambda)$, see Ref. [4] for the detailed calculation).

The resulting damping coefficient for the leading order of ω and d is

$$\Gamma = \frac{11}{64\mu_0|\omega|d} \langle F(X) \rangle^2. \quad (33)$$

The above expression is universal to any types of interaction for the leading order of ω . In fact, the elastic contribution is agnostic to the form of interaction, the characteristic of which we named *universality* in Ref. [4]. To see this, let us consider the locations of the singularities at $\omega \rightarrow 0$; the singularities are approaching to $k_{\parallel} = 0$ as $\omega \rightarrow 0$. This means the Green's function behaves like a delta function, and therefore the interaction has to be evaluated at $k_{\parallel} = 0$. By Eq. (28), $g(X, \mathbf{k}_{\parallel} = \mathbf{0}) = F(X)$ can be found; the damping coefficient does not depend on the form of the interaction. For detailed discussions and derivations of the universality of the elastic contribution, we refer the readers to Ref. [4].

TRANSVERSE VS. FULL SOLUTIONS

In the main text, the cases for arbitrary n are calculated with only the transverse waves considered. In Fig. 1, we present, for a few selected n values, a comparison between the full (transverse and longitudinal) and the transverse wave solutions. Note that in the plot, the damping coefficients calculated from the transverse solution are scaled by a factor

$$\frac{\Gamma^{\infty}}{\Gamma_{\text{T}}^{\infty}} = \frac{6.88\sqrt{2}}{\pi\sqrt{\pi}}, \quad (34)$$

which is nothing but the ratio of [Eq. (5)] in the main text to the viscous contribution in Eq. (20). From Fig. 1, it is clear that the transverse waves can capture the essential physics when it comes to the friction calculation.

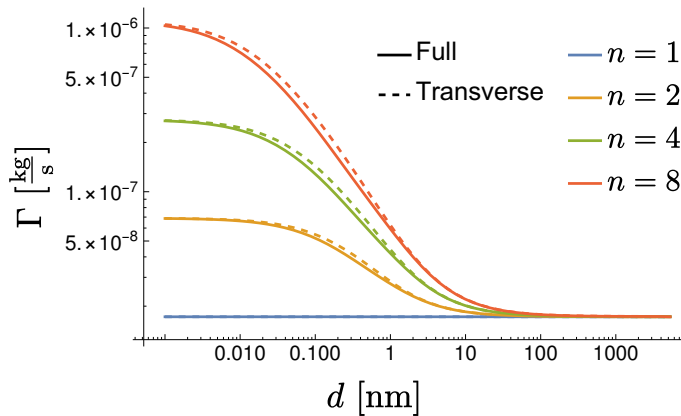


FIG. 1. Comparison between the full (transverse and longitudinal) and transverse solution calculations. Γ 's obtained from the transverse solution are scaled by the factor in Eq. (34).

FINDING THE PEAKS

For $\tilde{\eta} \ll 1$, the damping coefficient Γ exhibits peaks at $d \approx \lambda$, resulting from resonances of the excited waves. We identify that there are two types of resonances: body waves and surface waves. The former is due to interference of outgoing and reflected waves. The surface wave resonance, on the other hand, is related to the singularity of the Green's function in Fourier space ($\mathbf{k}_{\parallel}, \omega$) [16–18].

Let us begin with the peak of the surface wave. From Eq. (26), one finds that the position of singularity is at

$$k_s(\omega) = \frac{\sqrt{3 + \sqrt{3}}}{2} \frac{\omega}{c_{T0}(\omega)}. \quad (35)$$

The peak position of surface wave is thus

$$d^{\text{surface}}(\omega) = \frac{1}{2} \text{Re} \left\{ \frac{2\pi}{k_s(\omega)} \right\}. \quad (36)$$

The peaks of body waves can be found by considering the plane waves, i.e., evaluating the Green's function at $\mathbf{k}_{\parallel} = \mathbf{0}$,

$$G(\mathbf{0}, d, \omega) = \begin{cases} \frac{1}{\rho_0 c_{T0}} \tan\left(\frac{d\omega}{c_{T0}}\right) & n = 0 \\ -\frac{1}{\rho_0 c_{T0}} \cot\left(\frac{d\omega}{c_{T0}}\right) & n \rightarrow \infty, \end{cases} \quad (37)$$

from which the peak positions are obtained,

$$d_m^{\text{body}}(\omega) = \begin{cases} \frac{\pi c'_{T0}}{\omega} \left(\frac{1}{2} + m\right) & n = 0 \\ \frac{\pi c'_{T0}}{\omega} (1 + m) & n \rightarrow \infty, \end{cases} \quad m \in \{0, 1, 2, \dots\} \quad (38)$$

Figures 2 (a) and (b) show the peak positions for $n = 0$ and $n \rightarrow \infty$, respectively. The detected peak positions agree with our predictions as shown in the subsequent plots. Note that in Fig. 2 (b) we do not observe the plateau from the viscous contribution before the peaks. This is because $\tilde{\eta}$ and Q are inversely related to each other, resulting in $lQ \approx \lambda$; the peaks occur before the first plateau of the viscous contribution fully establishes.

DEFINING THE REGIMES IN [FIG. 5] IN THE MAIN TEXT

The scaling behavior of Γ can be understood by studying $\lim_{d \rightarrow 0} \Gamma$ and Γ^{∞} ,

$$\frac{\lim_{d \rightarrow 0} \Gamma}{\Gamma^{\infty}} = \frac{n^3 \zeta^{\text{ela}} + n^2 \zeta^{\text{vis}} \tilde{\eta}}{\zeta^{\text{ela}} + \zeta^{\text{vis}} \tilde{\eta}}. \quad (39)$$

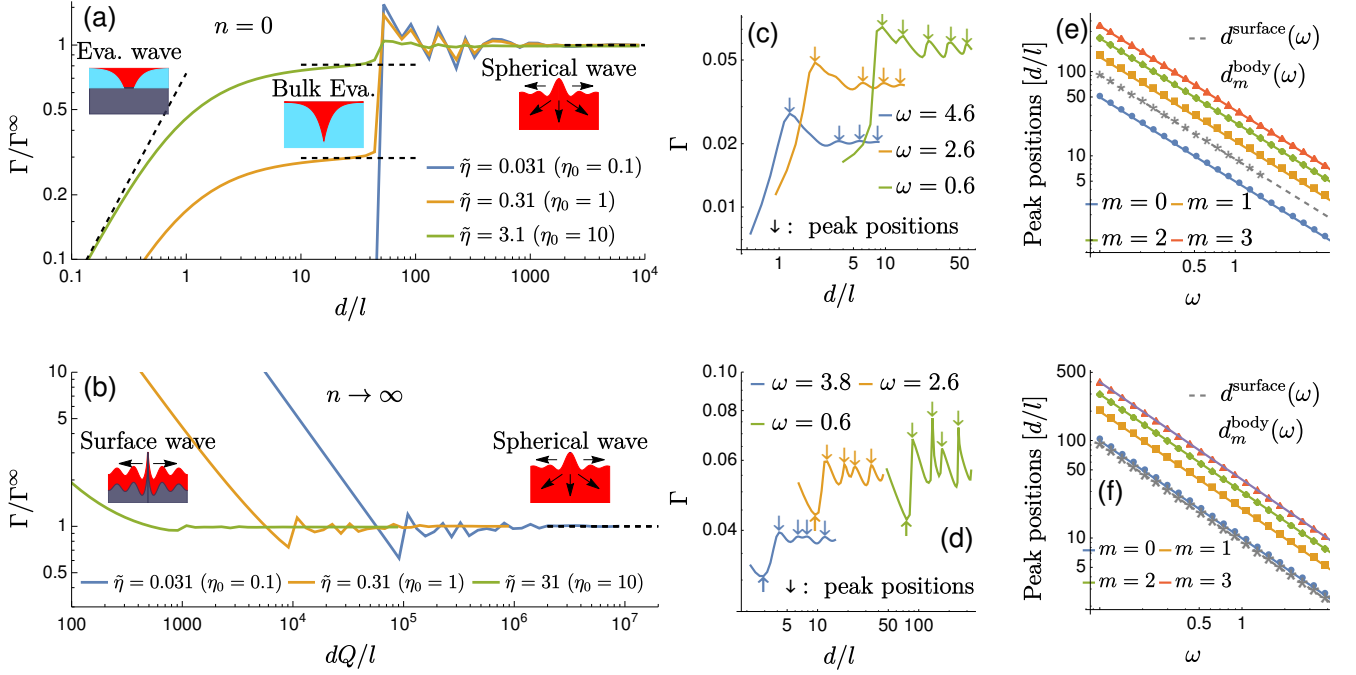


FIG. 2. (a) and (b): The damping coefficient Γ as a function of the depth of the first layer d for $n = 0$ (a) and $n \rightarrow \infty$ (b). The solid lines are numerical evaluations of the friction, whereas the black dashed lines are the asymptotes. The parameters are $\kappa = 1$, $l = 1$, $\omega = 0.1$, $n_A = 1$, $\rho = 1$, and $\mu = 10$, resulting in $\lambda/l \approx 200$. (c) and (d): A closer look of the damping coefficient near the peak positions with different values of ω at $\tilde{\eta} = 0.31$. (e) and (f): The first few peak positions as a function of ω at $\tilde{\eta} = 0.31$. The points are the detected peak positions from the numerical evaluations, and the lines are the exact peak positions.

Keep in mind that $\zeta^{\text{ela}}/\zeta^{\text{vis}} \approx 1$. The numerator is the damping coefficient of the substrate and the denominator that of the coating. To begin with, let us consider the numerator, from which a separating line

$$n = \tilde{\eta} \quad (40)$$

can be defined. If $n \gg \tilde{\eta}$, the elastic contribution of the substrate is much larger than the viscous contribution of the substrate.

Another line can be found when comparing the elastic contribution of the substrate with the viscous contribution of the coating,

$$n = \sqrt[3]{\tilde{\eta}}. \quad (41)$$

If $\sqrt[3]{\tilde{\eta}} \lesssim n \lesssim \tilde{\eta}$, one finds $\zeta^{\text{vis}}\tilde{\eta} \lesssim \zeta^{\text{ela}}n^3$; the viscous contribution of the coating is smaller than the elastic contribution of the substrate. Because the latter decays at a slow rate $d \approx Ql$, it is visible as shown in [Fig. 3] for $n = 100$ in the main text. Another case is when $\sqrt[3]{\tilde{\eta}} \lesssim n \lesssim 1$. The elastic contribution of the substrate is larger than the viscous contribution of the coating. In this case, the damping coefficient remains constant until $d \approx \lambda$.

Comparing the viscous contribution of the substrate to the elastic contribution of the coating defines yet another line,

$$n = \sqrt{\tilde{\eta}^{-1}}. \quad (42)$$

A case of interest would be $1 \lesssim \tilde{\eta} \lesssim n^{-2}$, where the viscous contribution of the substrate is much larger than the elastic contribution of the coating. This should result in two plateaus, one from the viscous contribution of the coating at $d \approx Ql$, the other from the elastic contribution at $d \approx \lambda$ similar to those seen in Fig. 2 (a). However, this regime is inaccessible since Q becomes inevitably large for small $\tilde{\eta}$ so that Ql becomes comparable to or larger than λ as discussed above. The line defined by Eq. (42) is thus not shown in [Fig. 5] in the main text.

GENERALIZING [EQ. (8)] IN THE MAIN TEXT

Even if the assumptions of n being real and $\rho_0 = \rho_1$ are relaxed, one can still gain useful insights into the scaling behavior of friction by constructing an equation similar to [Eq. (8)] in the main text (or Eq. (39) here in SM). This can be done by finding and comparing the bulk damping coefficients of the substrate and the coating from [Eq. (3)] in the main text,

$$\frac{\lim_{d \rightarrow 0} \Gamma}{\Gamma^\infty} = n'^3 \frac{\rho_0}{\rho_1} \left(\frac{\zeta^{\text{ela}} + n' \zeta^{\text{vis}} \frac{\eta_1}{c'_{T0} \rho_1 l}}{\zeta^{\text{ela}} + \zeta^{\text{vis}} \frac{\eta_0}{c'_{T0} \rho_0 l}} \right) \quad (43)$$

with $\text{Re}\{n\} = n' + \mathcal{O}(\omega^3) = c'_{T0}/c'_{T1} + \mathcal{O}(\omega^3)$.

* miru.lee@uni-goettingen.de

† matthias.kruger@uni-goettingen.de

- [1] R. Kubo, M. Toda, and N. Hashitsume, *Statistical physics II: nonequilibrium statistical mechanics*, Vol. 31 (Springer Science & Business Media, Berlin, 2012).
- [2] R. Zwanzig, *Nonequilibrium statistical mechanics* (Oxford University Press, Oxford, 2001).
- [3] M. Krüger and C. Maes, *Journal of Physics: Condensed Matter* **29**, 064004 (2016).
- [4] M. Lee, R. L. C. Vink, C. A. Volkert, and M. Krüger, *Physical Review B* **104**, 174309 (2021).
- [5] W. Eckhardt, *Physical Review A* **29**, 1991 (1984).
- [6] M. Krüger, T. Emig, and M. Kardar, *Physical Review Letters* **106**, 210404 (2011).
- [7] M. Krüger, G. Bimonte, T. Emig, and M. Kardar, *Physical Review B* **86**, 115423 (2012).
- [8] E. M. Lifshitz and L. P. Pitaevskii, *Statistical physics: theory of the condensed state*, Vol. 9 (Elsevier, Oxford, 2013).
- [9] G. Agarwal, *Physical Review A* **11**, 230 (1975).
- [10] C. M. Van Vliet, *Equilibrium And Non-equilibrium Statistical Mechanics (New And Revised Printing)* (World Scientific Publishing Company, 2008).
- [11] L. Landau, E. Lifshitz, J. Sykes, and W. Reid, *Theory of elasticity: Volume 7 of course of theoretical physics*, Vol. 7 (Elsevier, Oxford, 1986).
- [12] W. N. Findley, J. S. Lai, and K. Onaran, *Creep and Relaxation of Nonlinear Viscoelastic Materials, with an Introduction to Linear Viscoelasticity* (North-Holland Publishing Company, New York, N.Y., 2013).
- [13] E. Lee, *Quarterly of Applied Mathematics* **13**, 183 (1955).
- [14] R. D. Mindlin, *physics* **7**, 195 (1936).
- [15] L. M. Brekhovskikh, *Waves in layered media* (Academic Press, New York, 1980).
- [16] B. N. J. Persson and R. Ryberg, *Physical Review B* **32**, 3586 (1985).
- [17] A. I. Volokitin, B. N. J. Persson, and H. Ueba, *Physical Review B* **73**, 165423 (2006).
- [18] B. N. J. Persson, E. Tosatti, D. Fuhrmann, G. Witte, and C. Wöll, *Physical Review B* **59**, 11777 (1999).